(PVR2500, Perception). By tracing the dendrites in each sublamina, we obtained the dendritic field limits. The on and off sublamina were imaged by adjusting the depth of focus. In Figs 1 and 2, the extent of the on and off sublaminas are represented by light grey or black outlines, respectively.

Space–time alignment

We obtained Fig. 1d and e by correlating the spatial position of the dendritic field of the DS cell with the time response of the input currents. The position of the stimulus was known at all points in time and could therefore be aligned with the position of the dendrites. The horizontal scale of the figure was adjusted using the stimulus velocity such that the scale bar represents both 300 μm and 1 s. Therefore, any vertical line through the figure would give the position of the leading (Fig. 1d) or trailing (Fig. 1e) edge of the stimulus and the corresponding response magnitudes. The current trace in Fig. 1e is reversed to take into account the right-to-left stimulus movement.

Confocal reconstruction

After the whole-cell patch-clamp recordings, the retinas were fixed, permeabilized and incubated with streptavidin-conjugated Alexa Fluor 488 conjugate to stain the neurobiotin-filled cells. During the double patch experiments, the starburst cell pipette additionally contained Lucifer Yellow (lithium salt, Molecular Probes), which was recognized with a rabbit antibody against Lucifer Yellow (Chemicon International; used at a dilution of 1:100) and visualized with a Rhodamine-Red-conjugated donkey antibody against rabbit IgG (Jackson ImmunoResearch; used at a dilution of 1:200). Images of the whole-mount retina were taken at two different wavelengths (488 nm for ganglion cell morphology, 568 nm to image the starburst cell) on a Zeiss LSM 510 confocal microscope. We determined the relative amount of co-fasciculation between recorded starburst and DS cells by dividing the length of co-fasciculating processes by the total length of starburst dendrites in the region of overlap.

Received 6 June; accepted 2 September 2002; doi:10.1038/nature01179.

1. Barlow, H. B. & Hill, R. M. Selective sensitivity to direction of movement in ganglion cells of rabbit retina. *Science* **139,** 412–414 (1963).
2. Barlow, H. B. & Levick, W. R. Mechanism of directionally selective units in rabbits retina. *J. Physiol. (Lond.)* **178,** 477–504 (1965).
3. Vaney, D. I., He, S., Taylor, W. R. & Levick, W. R. *Motion Vision—Computational, Neural, and Ecological Constraints* (ed. Zeil, J.) 13–56 (Springer, Berlin, 2001).
4. Kittila, C. A. & Massey, S. C. Pharmacology of directionally selective ganglion cells in the rabbit retina. *J. Neurophysiol.* **77,** 675–689 (1997).
5. Caldwell, J. H., Daw, N. W. & Wyatt, H. J. Effects of picrotoxin and strychnine on rabbit retinal ganglion-cells—lateral interactions for cells with more complex receptive fields. *J. Physiol. (Lond.)* **276,** 277–298 (1978).
6. Famiglietti, E. V. Dendritic Costratification of on and on-off directionally selective ganglion-cells with starburst amacrine cells in rabbit retina. *J. Comp. Neurol.* **324,** 322–335 (1992).
7. Vaney, D. I. & Pow, D. V. The dendritic architecture of the cholinergic plexus in the rabbit retina: selective labeling by glycine accumulation in the presence of sarcosine. *J. Comp. Neurol.* **421,** 1–13 (2000).
8. O'Malley, D. M., Sandell, J. H. & Masland, R. H. Corelease of acetylcholine and GABA by the starburst amacrine cells. *J. Neurosci.* **12,** 1394–1408 (1992).
9. Brecha, N., Johnson, D., Peichl, L. & Wässle, H. Cholinergic amacrine cells of the rabbit retina contain glutamate-decarboxylase and γ-aminobutyrate immunoreactivity. *Proc. Natl Acad. Sci. USA* **85,** 6187–6191 (1988).
10. Vaney, D. I. & Young, H. M. GABA-like immunoreactivity in cholinergic amacrine cells of the rabbit retina. *Brain Res.* **438,** 369–373 (1988).
11. He, S. G. & Masland, R. H. Retinal direction selectivity after targeted laser ablation of starburst amacrine cells. *Nature* **389,** 378–382 (1997).
12. Yoshida, K. *et al.* A key role of starburst amacrine cells in originating retinal directional selectivity and optokinetic eye movement. *Neuron* **30,** 771–780 (2001).
13. Taylor, W. R., He, S. Y., Levick, W. R. & Vaney, D. I. Dendritic computation of direction selectivity by retinal ganglion cells. *Science* **289,** 2347–2350 (2000).
14. Borg-Graham, L. J. The computation of directional selectivity in the retina occurs presynaptic to the ganglion cell. *Nature Neurosci.* **4,** 176–183 (2001).
15. Famiglietti, E. V. Starburst amacrine cells and cholinergic neurons—mirror-symmetric on and off amacrine cells of rabbit retina. *Brain Res.* **261,** 138–144 (1983).
16. Masland, R. H., Mills, J. W. & Hayden, S. A. Acetylcholine-synthesizing amacrine cells—identification and selective staining by using autoradiography and fluorescent markers. *Proc. R. Soc. Lond. Ser. B* **223,** 79–100 (1984).
17. Masland, R. H. & Mills, J. W. Autoradiographic identification of acetylcholine in the rabbit retina. *J. Cell Biol.* **83,** 159–178 (1979).
18. Linn, D. M., Blazynski, C., Redburn, D. A. & Massey, S. C. Acetylcholine-release from the rabbit retina mediated by kainate receptors. *J. Neurosci.* **11,** 111–122 (1991).
19. Masland, R. H. & Ames, A. Responses to acetylcholine of ganglion-cells in an isolated mammalian retina. *J. Neurophysiol.* **39,** 1220–1235 (1976).
20. Famiglietti, E. V. Starburst amacrine cells—morphological constancy and systematic variation in the anisotropic field of rabbit retinal neurons. *J. Neurosci.* **5,** 562–577 (1985).
21. Peters, B. N. & Masland, R. H. Responses to light of starburst amacrine cells. *J. Neurophysiol.* **75,** 469–480 (1996).
22. Borg-Graham, L. J. & Grzywacz, N. M. *Single Neuron Computation* (ed. Zornetzer, S. F.) 347–375 (Academic, London, 1992).
23. Poznanski, R. R. Modeling the electrotonic structure of starburst amacrine cells in the rabbit retina—a functional interpretation of dendritic morphology. *Bull. Math. Biol.* **54,** 905–928 (1992).
24. Vaney, D. I. *Progress in Retinal Research* (ed. Chader, G. J.) 49–100 (Oxford, Pergamon, 1990).
25. Famiglietti, E. V. Synaptic organization of starburst amacrine cells in rabbit retina—analysis of serial thin-sections by electron-microscopy and graphic reconstruction. *J. Comp. Neurol.* **309,** 40–70 (1991).
26. Euler, T., Detwiler, P. B. & Denk, W. Directionally selective calcium signals in dendrites of starburst amacrine cells. *Nature* **418,** 845–852 (2002).
27. Mills, S. L. & Massey, S. C. Morphology of bipolar cells labelled by DAPI in the rabbit retina. *J. Comp. Neurol.* **321,** 133–149 (1992).
28. Roska, B. & Werblin, F. Vertical interactions across ten parallel, stacked representations in the mammalian retina. *Nature* **410,** 583–587 (2001).

Acknowledgements We thank K. Okazaki for help with confocal preparations and image analysis; J. Hurtado, R. Kramer and C. Kretschmann for discussion; and H. Barlow, R. Froemke, E. Isacoff, X. Ren and R. Zucker for comments on the manuscript. This work was supported by grants from the Office of Naval Research, the National Eye Institute, and an NIH training grant in Vision Science to the University of California Berkeley (S.F.).

Competing interests statement The authors declare that they have no competing financial interests.

Correspondence and requests for materials should be addressed to F.W. (e-mail: werblin@socrates.berkeley.edu)

Multiple forms of synaptic plasticity triggered by selective suppression of activity in individual neurons

Juan Burrone, Michael O'Byrne & Venkatesh N. Murthy

Department of Molecular & Cellular Biology, Harvard University, Cambridge, Massachusetts 02138, USA

The rules by which neuronal activity causes long-term modification of synapses in the central nervous system are not fully understood. Whereas competitive or correlation-based rules result in local modification of synapses, homeostatic modifications allow neuron-wide changes in synaptic strength, promoting stability[1,2]. Experimental investigations of these rules at central nervous system synapses have relied generally on manipulating activity in populations of neurons[1,3–6]. Here, we investigated the effect of suppressing excitability in single neurons within a network of active hippocampal neurons by overexpressing an inward-rectifier potassium channel. Reducing activity in a neuron before synapse formation leads to a reduction in functional synaptic inputs to that neuron; no such reduction was observed when activity of all neurons was uniformly suppressed. In contrast, suppressing activity in a single neuron after synapses are established results in a homeostatic increase in synaptic input, which restores the activity of the neuron to control levels. Our results highlight the differences between global and selective suppression of activity, as well as those between early and late manipulation of activity.

Activity is thought to play a role in the formation and modification of neural circuits[3,7]. The specific manner in which activity modifies synaptic strength remains a matter of speculation, and is controversial even in relatively well-studied systems[8–12]. Two general classes of synaptic modification have emerged as targets of concerted investigation. Hebbian modification has been studied at the level of single neurons or single synapses over a timescale of hours[13,14]. In contrast, homeostatic modifications have been studied over longer timescales, but have involved uniform changes in activity in entire networks of central neurons[4,5,15]. The relation between these two rules of synaptic modification has not been studied experimentally.

We sought to determine the consequences of chronic suppression of activity in single neurons within an active network (Fig. 1a). To this end, we used the inward-rectifier potassium channel Kir2.1, which has been used to suppress excitability in mammalian superior cervical ganglion cells and chick hair cells[16,17]. Overexpression of this channel hyperpolarizes the neuron and decreases its resting

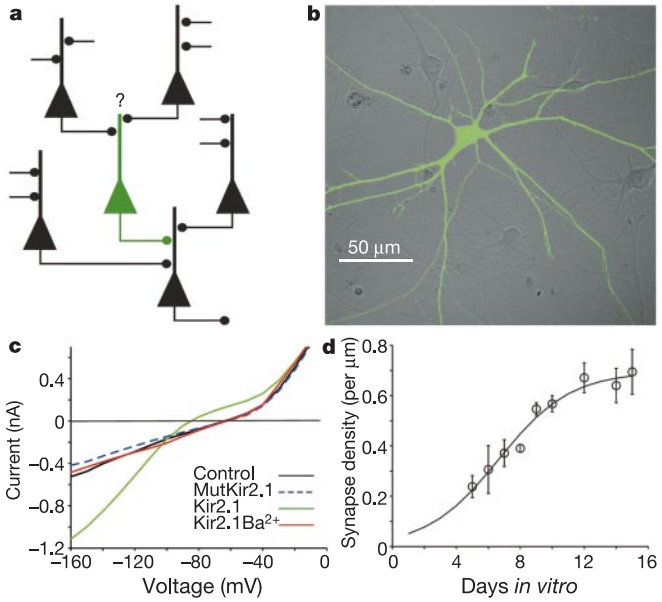

Figure 1 Overexpression of Kir2.1 in individual neurons depresses excitability. **a**, Examination of the long-term consequences of suppressing activity in a single cell (green) embedded in a network of active cells (black). **b**, Superposition of fluorescence and transmitted light images showing the normal morphology of a pyramidal neuron expressing Kir2.1 and EGFP. Transfection was on day 10, and images were obtained on day 14. **c**, Current–voltage relationship showing that cells overexpressing Kir2.1 have significantly larger inward-rectifying currents than mutKir2.1 or untransfected control cells; this additional current was abolished by extracellular Ba^{2+}. **d**, Time course of synapse formation in cultures. The number of active presynaptic terminals was measured using the vesicle dye FM4-64, and each point is an average of at least three cells. The continuous line is a sigmoidal function with half-maximum at about 6.5 days.

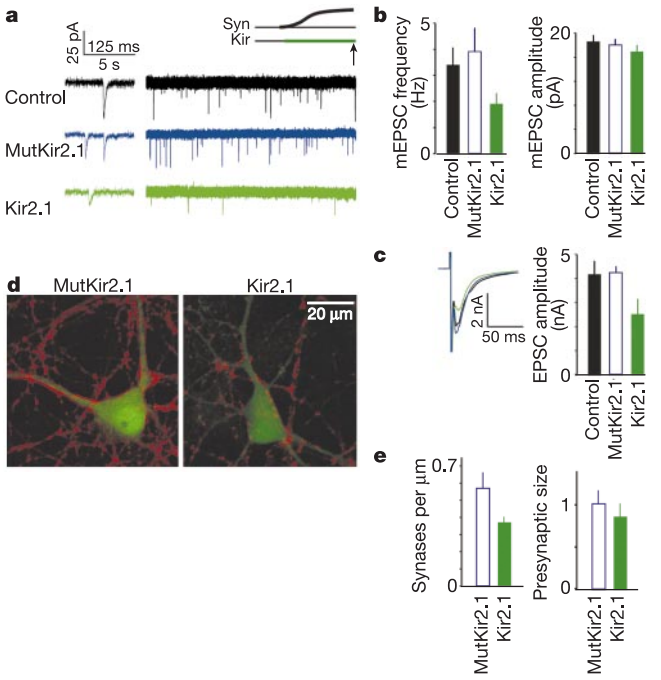

Figure 2 Suppression of activity before synapse formation leads to a reduction in synaptic input. **a**, Examples of recordings from neurons expressing Kir2.1 or mutKir2.1, and an untransfected control neuron on day 14. To the left of each trace, a small segment is shown at expanded timescale to indicate typical miniature excitatory postsynaptic currents (mEPSCs). The top right inset shows the experimental time line with time course of synapse formation (Syn), duration of Kir2.1 overexpression (green) and time of recording (arrow). **b**, The average rate of mEPSCs in cells expressing Kir2.1 is lower than in control or mutKir2.1 cells ($P < 0.005$), but the quantal amplitudes are not different. **c**, Examples of action-potential-evoked EPSCs recorded from single Kir2.1 (green), mutKir2.1 (blue) and control (black) cells. The average EPSC was significantly lower in Kir2.1 cells than in the other two ($P < 0.01$). **d**, Superimposed images of the green (EGFP) and red (FM4-64) fluorescence from a mutKir2.1 cell and Kir2.1 cell taken at the same instrument settings. **e**, The average synapse density for Kir2.1 neurons was significantly smaller than that of mutKir2.1 cells ($P < 0.01$). The average intensity of the individual synapses (normalized), a measure of the presynaptic vesicle pool size, was smaller for Kir2.1 neurons ($P < 0.05$).

membrane resistance. Once the spike threshold is reached, however, the Kir2.1 current contributes negligibly to the spike waveform. Therefore, expression of Kir2.1 causes the neuron to be less excitable than neighbouring neurons, leading to a persistent imbalance in activity.

We used a bicistronic construct made from coding sequences of human Kir2.1 and enhanced green fluorescent protein (EGFP) separated by an internal ribosome entry site (IRES) to transfect hippocampal neurons in culture (ref. 16; Fig. 1b). To control for nonspecific effects caused by overexpression of Kir2.1, we carried out parallel experiments using a non-conducting mutant version of Kir2.1 (mutKir2.1) with the pore region amino acid motif GYG mutated to AAA. The low efficiency of transfection using the calcium phosphate method[18] allowed us to minimize interaction between multiple inactivated cells. Neurons overexpressing Kir2.1 exhibited prominent inward-rectifying currents (Fig. 1c), and their resting potential and input resistance were significantly below that of control and mutant Kir2.1-expressing cells (Table 1; $P < 0.01$). These differences were abolished by low concentrations (300 µM) of extracellular Ba^{2+} (Fig. 1c and Table 1). In current-clamp recordings, larger currents were required to bring Kir2.1 neurons to threshold (data not shown). Expression of the additional current reached a stable level within 48 h, and was maintained for several days (see Supplementary Information). Hippocampal networks in dissociated culture normally maintain action-potential firing at low rates owing to their recurrent connections and spontaneous vesicle release. If expression of Kir2.1 leads to decreased excitability, the average firing rates should be lower than normal. As predicted, 24 h after transfection spike-firing rates measured using cell-attached patch-clamp recording were significantly reduced (control, 0.51 ± 0.19 Hz; Kir2.1, 0.08 ± 0.06 Hz, $P < 0.01$, Kolmogorov–Smirnoff test, which is used for all comparisons below).

Table 1 **Passive parameters**

Cell treatment	Resting potential (mV)*	Input resistance (MΩ)
Control	−65 ± 2.1 (10)	166 ± 11 (10)
MutKir2.1	−64 ± 0.6 (10)	216 ± 12 (10)
Kir2.1	−73 ± 2.3 (13)	63 ± 25 (13)
Kir2.1 + Ba^{2+}	−63 ± 1.4 (13)	219 ± 14 (13)

The number of cells is indicated in parentheses.
*Corrected for junction potential.

Previous experiments have suggested that synapses can form in the absence of activity in dissociated cultures[4,19–22]. In those experiments, activity was blocked globally, affecting all neurons in culture. At the vertebrate neuromuscular junction the effect of local manipulation of activity is markedly different from that of global manipulation[23]. Therefore, we wondered whether more selective manipulation of activity might uncover mechanisms that are invisible to uniform suppression of activity. To ensure proper timing of suppression of excitability, we first characterized the time course of synapse formation in our cultures by labelling active presynaptic terminals with styryl dyes[24]. Functional presynaptic terminals could be detected as early as 4 days *in vitro*, but a rapid increase in the number of synapses occurred between day 6 and 10 (Fig. 1d). After day 10, the density of synapses did not increase

Table 2 **Synaptic parameters**

Cell treatment	mEPSC frequency (Hz)	mEPSC amplitude (pA)	Synapse density (μm^{-1})	Presynaptic pool size (normalized)
Control	3.4 ± 0.65 (21)	18.6 ± 1.02 (21)	–	–
Kir2.1 (early)	1.9 ± 0.41 (37)	16.9 ± 1.07 (37)	0.37 ± 0.034 (8)	0.83 ± 0.14 (8)
Kir2.1 (early) + Ba^{2+}	1.9 ± 0.56 (9)	15.7 ± 1.78 (9)	–	–
MutKir2.1	3.9 ± 0.91 (23)	18.0 ± 0.97 (23)	0.57 ± 0.093 (6)	1.00 ± 0.15 (6)
Kir2.1 (early) + TTX	11.7 ± 4.13 (13)	22.6 ± 3.01 (13)	0.53 ± 0.029 (6)	1.22 ± 0.10 (6)
MutKir2.1 (early) + TTX	–	–	0.59 ± 0.029 (6)	1.15 ± 0.1 (6)
Control + TTX	12.1 ± 3.20 (13)	22.5 ± 2.03 (13)	–	–
Kir2.1 (late)	5.7 ± 1.01 (15)	17.7 ± 1.5 (15)	0.64 ± 0.081 (6)	1.24 ± 0.14 (6)

The number of cells is indicated in parentheses. Early, transfection before synapse formation; late, after synapse formation.

significantly. The rate of miniature excitatory postsynaptic currents (mEPSCs) seems to undergo a similar increase and stabilization[21].

To examine the effect of reducing excitability of a neuron before synapse formation, we transfected neurons 2–5 days *in vitro*, when synapse density was low. We then used whole-cell patch-clamp recordings to measure the frequency and amplitude of α-amino-3-hydroxy-5-methyl-4-isoxazole propionic acid (AMPA) receptor-mediated mEPSCs on day 14 (Fig. 2). Compared with control or mutKir2.1 neurons, Kir2.1-transfected neurons had fewer mEPSCs (Fig. 2a, b; $P < 0.005$) whose average amplitude was not significantly different (Fig. 2b and Table 2; $P > 0.1$). We next tested whether the reduced rate of mEPSCs in cells transfected with Kir2.1 led to smaller evoked synaptic currents. To obtain a measure of the total synaptic input to a single neuron, we used extracellular stimulation to evoke action potentials synchronously in all neurons. Evoked EPSCs were smaller on average in cells expressing Kir2.1 than in control or mutKir2.1 cells (Fig. 2c; Kir2.1, 2.50 ± 0.64 nA; control, 4.16 ± 0.56 nA; mutKir2.1, 4.24 ± 0.26 nA, $P < 0.01$, $n = 6$ each), suggesting a reduced functional input to neurons overexpressing Kir2.1.

To determine whether the decrease in the number of functional synaptic inputs was due to a reduction in the number of synapses, we measured the density of active presynaptic terminals labelled with FM4-64 (Fig. 2d). We found significantly fewer functional presynaptic boutons terminating on Kir2.1 neurons than on mutKir2.1 neurons (Fig. 2e and Table 2; $P < 0.001$). The functional size of the fewer synapses made on Kir2.1 neurons, estimated from the intensity of FM4-64 staining, was smaller than those made on mutKir2.1 neurons (Fig. 2e and Table 2; $P < 0.05$). Therefore, fewer synapses were made onto neurons with reduced excitability, and these synapses were presumably weaker than control synapses because of their smaller presynaptic vesicle pool.

The reduction in synaptic inputs to the Kir2.1-expressing cells might be due to a nonspecific reduction of cell viability or function. Several observations argue against this possibility. First, the use of the pore mutant Kir2.1 helped us rule out effects that are independent of the ionic conduction of the channel. Second, the intrinsic electrical properties of transfected neurons were not altered beyond that expected from the expression of potassium currents—for example, action potentials were intact, and the membrane potential and resting conductance were restored to control levels on addition of extracellular Ba^{2+}. Third, the axons of transfected neurons had normal presynaptic terminals, as judged by the expression of vesicle-associated membrane protein (VAMP) fused to EGFP[25] (see Supplementary Information). The fourth and most compelling argument against nonspecific effects in transfected neurons is that we could prevent the reduction in synaptic inputs by silencing the entire network of neurons using tetrodotoxin (TTX; see below).

Does the reduction in synaptic inputs to the less active neuron result from a relative reduction in activity compared with neighbouring active neurons, or is it due to an absolute reduction in activity? To distinguish between these possibilities, we blocked sodium action potentials in the entire network using TTX for 5–9 days before recordings were done (Fig. 3a). Although the transfected neuron will continue to have a lower resting potential than its neighbours, none of the neurons will produce action potentials. We found that within days of the global activity blockade, transfected neurons regained synaptic inputs and resembled their untransfected neighbours (Fig. 3a). The rates of mEPSCs increased uniformly across all neurons (Fig. 3b; $P < 0.001$), consistent with our previous findings that presynaptic vesicle pools are larger in TTX-treated cultures[26]. The amplitudes of mEPSCs were also larger (Fig. 3b; $P < 0.01$), as seen for cortical neurons[5]. The number of functional presynaptic boutons terminating on Kir2.1 neurons was indistinguishable from those on mutKir2.1 neurons (Fig. 3c, d). Furthermore, TTX treatment increased the size of the total recycling vesicle pool in boutons terminating on both Kir2.1 and mutKir2.1 neurons (Fig. 3d; see also ref. 26). Although it is possible that blocking spike activity using TTX activates an entirely different cellular programme, these results nevertheless indicate that it is not simply the lack of activity that results in fewer inputs to transfected neurons. One hypothesis is that the decrease in synaptic input observed in Kir2.1 neurons without TTX is triggered by the difference in activity levels between different neurons.

Previous studies in dissociated cultures have found that global block of activity using TTX leads to an increase in quantal amplitude[5], presynaptic release probability[26], spontaneous release[27]

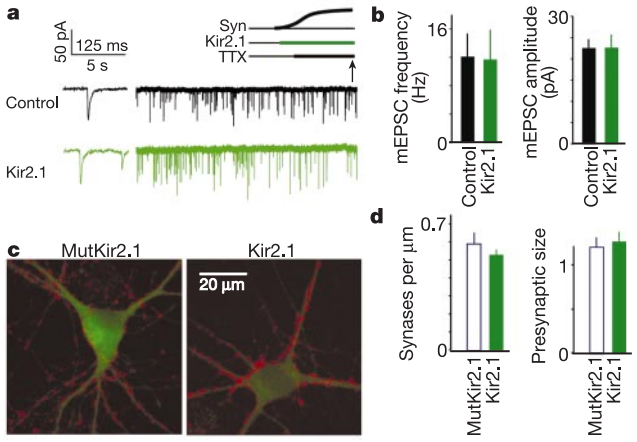

Figure 3 Blocking activity uniformly using TTX equalizes synaptic inputs to Kir2.1 and control cells. **a**, Sample recordings from a neuron transfected with Kir2.1 and a control neuron, both grown in TTX for 3 days. The experimental time line is shown in the top right inset. **b**, The frequency of mEPSCs for cells expressing Kir2.1 and for control neurons increase substantially after TTX treatment, but no difference was observed between Kir2.1 and control neurons in TTX ($P > 0.5$). Similarly, the average amplitudes of mEPSCs increased after TTX treatment ($P < 0.005$), but no difference was observed between Kir2.1 and control cells after TTX treatment ($P > 0.5$). **c**, Sample images illustrating that cells transfected with Kir2.1 gain active presynaptic boutons after TTX treatment. **d**, The density of presynaptic terminals on Kir2.1 cells was similar to those on mutKir2.1 neurons ($P > 0.5$). The average presynaptic vesicle pool size was similar ($P > 0.2$) for Kir2.1 and mutKir2.1 cell synapses after TTX treatment, but both had larger vesicle pools compared with non-TTX cells ($P < 0.01$).

and the ultrastructurally determined size of the synapse[26]. At the *Drosophila* neuromuscular junction, overexpression of Kir2.1 in muscle triggers a homeostatic increase in transmitter release[28]. We wondered what effect silencing a single neuron would have on established rather than developing synapses, and how this might compare with the global blockade of activity using TTX. To investigate this, we transfected neurons with Kir2.1 at 10 days *in vitro*, when synapse number is close to steady state (Fig. 1d). We confirmed that expression of Kir2.1 led to a reduction in the resting membrane potential and membrane resistance. In contrast to suppression of excitability before synapse formation, we found that late suppression led to a significant increase in the frequency of mEPSCs (Fig. 4a, b; $P < 0.005$), whereas the quantal amplitude was not different (Fig. 4b; $P > 0.1$). The increased rate of mEPSCs in cells transfected with Kir2.1 was accompanied by an increase in the total evoked synaptic currents (Fig. 4c; Kir2.1, 1.76 ± 0.4 nA; control, 1.38 ± 0.35 nA; $n = 6$, $P < 0.05$), suggesting a larger functional input to neurons overexpressing Kir2.1. The modest increase in evoked release might be sufficient to overcome the effect of Kir2.1, which inactivates on depolarization. The effects of the global activity block on established synapses were larger than those caused by Kir2.1 (Fig. 3), perhaps reflecting the stronger block of activity by TTX compared with Kir2.1.

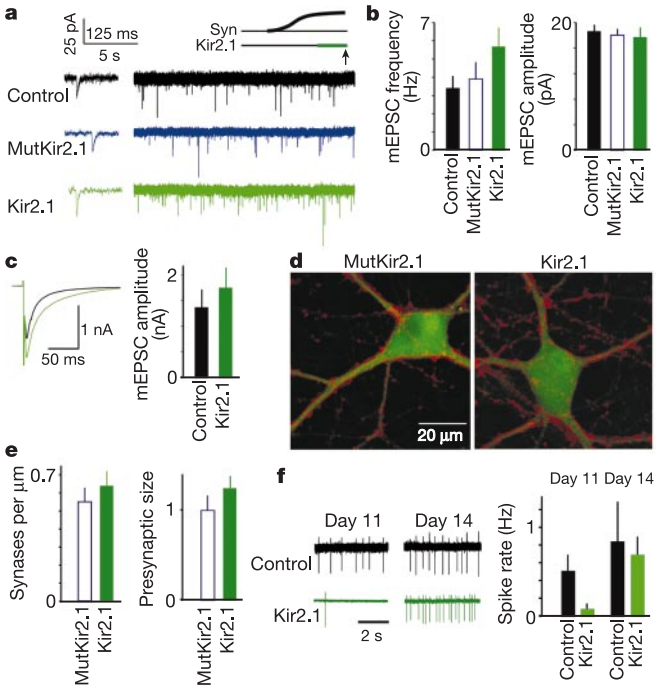

Figure 4 Suppression of excitability after synapse formation leads to a homeostatic increase in synaptic inputs. **a**, Example recordings of mEPSCs from neurons transfected with Kir2.1 or mutKir2.1. **b**, The average rate of mEPSCs in cells transfected with Kir2.1 was higher than those of control or mutKir2.1 neurons ($P < 0.005$), but the amplitudes were not different ($P > 0.2$). **c**, Evoked EPSCs recorded from a neuron transfected with Kir2.1 (green) and from a control neuron (black). The average EPSC was larger in Kir2.1 neurons ($P < 0.01$). **d**, Examples showing the similarity in the number of presynaptic boutons terminating on Kir2.1-transfected and mutKir2.1 neurons. **e**, The average density of presynaptic terminals was not significantly different between mutKir2.1 neurons and neurons expressing Kir2.1 ($P > 0.5$), but the intensity of individual boutons was larger for Kir2.1 neurons ($P < 0.05$). **f**, Increase in mEPSC rate restores firing rates of Kir2.1 neurons. One day after transfection, spike frequencies were significantly lower in Kir2.1 cells compared with control cells ($P < 0.01$). By day 14 (4 days after transfection) however, spike frequencies were similar in transfected and control cells ($P > 0.3$). Sample recordings of spikes are shown (left).

The number of presynaptic boutons terminating on Kir2.1 neurons was not significantly different from mutKir2.1 neurons (Fig. 4d, e). However, the total recycling pool of vesicles was larger in synapses terminating on Kir2.1 neurons (Fig. 4e; $P < 0.01$). Although the larger vesicle pool could explain the higher frequency of mEPSCs, we have not ruled out additional contributions from an increase in the number of synapses with detectable AMPA currents[29,30]. We next tested whether the increase in functional synaptic inputs could compensate for the decrease in intrinsic excitability of the Kir2.1 cells, and restore normal spike activity. One day after transfection, the spike firing rates in Kir2.1 cells were substantially reduced (Fig. 4f). Notably, over the next 3 days, the spike-firing rate returned to control levels (Fig. 4f; control, 0.84 ± 0.45 Hz; Kir2.1, 0.70 ± 0.21 Hz; $n = 8$, $P > 0.5$), presumably due to a compensatory increase in transmitter release. This normalization of firing rate was not observed in neurons whose activity was suppressed before synapse formation (mutKir2.1, 0.82 ± 0.23 Hz; Kir2.1, 0.30 ± 0.18 Hz; $n = 8$, $P < 0.01$ measured at day 9).

Using a relatively simple and accessible model system, we have uncovered a role for activity in the regulation of synaptic inputs to a neuron. Silencing a neuron before synapses are formed leads to a reduction in synaptic inputs to this less-excitable neuron, implying that axons, when faced with a choice of active or silent neurons, prefer to make synapses on more easily excited neurons. It remains to be determined whether the loss of synaptic inputs is due to a lack of synapse formation itself, or the inability to stabilize nascent synapses. In contrast to the effect of early reduction of excitability, we found that suppressing excitation after synapses are already in place led to a homeostatic increase in synaptic input strength. Although the mechanism underlying this increase might be similar to that seen after global block of activity[1,5,6,15], our experiments establish that the homeostatic increase is cell autonomous. Also, we find that the increase in synaptic inputs is quite precise and restores the frequency of action potential firing to control levels; such normalization of activity is not possible with TTX treatment. These results complement findings at the *Drosophila* neuromuscular junction, where overexpression of Kir2.1 in muscle fibres resulted in an increase in quantal content, without changes in quantal amplitude or synapse morphology[28].

Our experiments indicate that decreased neuronal activity can have multiple and widely different effects depending on the developmental stage of neuronal networks. The experimental system described here might enable the study of the mechanisms underlying the differential effects of early and late suppression of activity, as well as activity dependent, long-term synaptic plasticity in general. □

Methods

Culture and transfection

Neonatal hippocampal neurons (P0–P2) were cultured on glia feeder layers as described previously[26]. Density of neurons at time of analysis (14–15 days) was approximately 50 neurons per mm^2. Cells were transfected with the bicistronic EGFP–IRES–Kir2.1 construct[16] using the calcium phosphate transfection protocol[18]. As a control, we used channels with mutations in the pore residues, GYG to AAA, made using the Quikchange XL site-directed mutagenesis kit (Stratagene). The concentration of plasmid DNA was optimized empirically to produce robust transfection in a small number of individual neurons on each coverslip. Neurons were transfected on 2–5 days *in vitro*, or 10–11 days *in vitro*.

Electrophysiology

Patch-clamp recordings from cultured hippocampal neurons were performed with an Axopatch 200B amplifier. Electrodes, whose tip resistances were 4–7 MΩ, contained (in mM): 130 potassium gluconate, 10 NaCl, 1 EGTA, 0.133 $CaCl_2$, 2 $MgCl_2$, 10 HEPES, 3.5 MgATP, and 1 NaGTP. Extracellular perfusion medium contained (in mM): 136 NaCl, 2.5 KCl, 10 HEPES, 10 D-glucose, 2 $CaCl_2$, and 1.3 $MgCl_2$. Recordings were filtered at 2–5 kHz and were acquired at 5–10 kHz. For recording mEPSCs and current–voltage relationship, extracellular medium was supplemented with 50 µM picrotoxin and 0.5 or 1 µM TTX. Analysis of mEPSCs was performed using the MiniAnalysis program (Synaptosoft). To determine the effect of increased membrane permeability caused by Kir2.1 overexpression on mEPSC frequency and amplitude, in some experiments we compared recordings made

in the presence and absence of 300 μM extracellular Ba^{2+}. Current–voltage relations for transfected and control neurons were calculated by recording whole-cell currents under voltage clamp. Voltage steps in 10-mV increments were applied every 1 s. Evoked synaptic currents were recorded using pipettes whose internal solution was supplemented with QX-314 (4 mM), and in the presence of 50–100 μM picrotoxin in the extracellular medium to isolate excitatory synapses. Brief 1-ms pulses were applied to the entire field of neurons using platinum wires separated by about 5 mm. The applied voltage was systematically varied for each recording until the response amplitude became saturated, indicating reliable activation of all axons innervating the recorded neuron. Responses were measured at a holding potential of −70 mV. To record action-potential firing, without perturbing the intracellular environment, we used the cell-attached patch-clamp method. Pipettes similar to those for whole-cell recordings were used, and tight seals were obtained without break-in. Current recordings (under voltage clamp at −70 mV) allowed unambiguous discrimination of spikes with high signal-to-noise ratios.

FM4-64 imaging

To identify functional presynaptic terminals, we labelled recycling synaptic vesicles using 10 μM FM4-64 (Molecular Probes). Neurons were depolarized for 60 s using hyperkalaemic solution (in mM): 78.5 NaCl, 60 KCl, 10 HEPES, 10 D-glucose, 2 $CaCl_2$, 1.3 $MgCl_2$, 0.05 AP5 (D(-)-2-amino-5-phosphonovaleric acid), 0.005 CNQX (6-cyano-7-nitroquinoxaline-2,3-dione), and 0.001 TTX. Coverslips were then washed in regular extracellular medium without FM4-64 for 10 min before imaging to reduce the background fluorescence caused by non-internalized dye binding to the cell membrane. This protocol has been shown to provide an estimate of the total recycling pool of vesicles. Cells were then imaged in dye-free buffer containing blockers. Earlier experiments also included a de-staining step to release dye from vesicles, and images after de-staining were subtracted from the initial image. As the initial fluorescence and releasable fluorescence were strongly correlated, in most experiments we skipped the de-staining step. Image stacks (Z steps of 1 μm, 7–10 steps) were obtained using a confocal microscope (Olympus Fluoview attached to a BX50WI, × 40, 0.8NA water lens). EGFP and FM4-64 signals were acquired simultaneously using 488-nm excitation, and 510–550-nm band pass and 585 long-pass emission filters, respectively. Transmitted light images were taken separately to identify cell bodies and processes of non-transfected neurons. We chose to measure the density of presynaptic terminals in the proximal regions of the dendrites (about 100 μm from the soma) as these could be identified unequivocally by the EGFP fluorescence. Image analysis was performed in a blind manner with respect to Kir2.1 and mutKir2.1 neurons. Individual puncta were identified manually after thresholding the images using a value that was 2 standard deviations above the background fluorescence. Analysis of fluorescence intensities was performed with custom-written routines in the MATLAB software environment[26].

Analysis

The values for all variables reported were estimated for each cell and averaged across all cells in each group. Errors are reported as standard error of the mean. The Kolmogorov–Smirnoff test was used for all statistical comparisons.

Received 16 July; accepted 23 October 2002; doi:10.1038/nature01242.

1. Turrigiano, G. G. & Nelson, S. B. Hebb and homeostasis in neuronal plasticity. *Curr. Opin. Neurobiol.* **10,** 358–364 (2000).
2. Abbott, L. F. & Nelson, S. B. Synaptic plasticity: taming the beast. *Nature Neurosci.* **3 Suppl.,** 1178–1183 (2000).
3. Katz, L. C. & Shatz, C. J. Synaptic activity and the construction of cortical circuits. *Science* **274,** 1133–1138 (1996).
4. Rao, A. & Craig, A. M. Activity regulates the synaptic localization of the NMDA receptor in hippocampal neurons. *Neuron* **19,** 801–812 (1997).
5. Turrigiano, G. G., Leslie, K. R., Desai, N. S., Rutherford, L. C. & Nelson, S. B. Activity-dependent scaling of quantal amplitude in neocortical neurons. *Nature* **391,** 892–896 (1998).
6. Liao, D., Zhang, X., O'Brien, R., Ehlers, M. D. & Huganir, R. L. Regulation of morphological postsynaptic silent synapses in developing hippocampal neurons. *Nature Neurosci.* **2,** 37–43 (1999).
7. Sanes, J. R. & Lichtman, J. W. Development of the vertebrate neuromuscular junction. *Ann. Rev. Neurosci.* **22,** 389–442 (1999).
8. Crowley, J. C. & Katz, L. C. Development of ocular dominance columns in the absence of retinal input. *Nature Neurosci.* **2,** 1125–1130 (1999).
9. Hubener, M. & Bonhoeffer, T. Eyes wide shut. *Nature Neurosci.* **2,** 1043–1045 (1999).
10. Lin, D. M. *et al.* Formation of precise connections in the olfactory bulb occurs in the absence of odorant-evoked neuronal activity. *Neuron* **26,** 69–80 (2000).
11. Zheng, C., Feinstein, P., Bozza, T., Rodriguez, I. & Mombaerts, P. Peripheral olfactory projections are differentially affected in mice deficient in a cyclic nucleotide-gated channel subunit. *Neuron* **26,** 81–91 (2000).
12. Zhao, H. & Reed, R. R. X inactivation of the OCNC1 channel gene reveals a role for activity-dependent competition in the olfactory system. *Cell* **104,** 651–660 (2001).
13. Luscher, C., Nicoll, R. A., Malenka, R. C. & Muller, D. Synaptic plasticity and dynamic modulation of the postsynaptic membrane. *Nature Neurosci.* **3,** 545–550 (2000).
14. Bi, G. Q. & Poo, M. M. Synaptic modification by correlated activity: Hebb's postulate revisited. *Ann. Rev. Neurosci.* **24,** 139–166 (2001).
15. Davis, G. W. & Bezprozvanny, I. Maintaining the stability of neural function: a homeostatic hypothesis. *Annu. Rev. Physiol.* **63,** 847–869 (2001).
16. Johns, D. C., Marx, R., Mains, R. E., O'Rourke, B. & Marban, E. Inducible genetic suppression of neuronal excitability. *J. Neurosci.* **19,** 1691–1697 (1999).
17. Holt, J. R. *et al.* Functional expression of exogenous proteins in mammalian sensory hair cells infected with adenoviral vectors. *J. Neurophysiol.* **81,** 1881–1888 (1999).
18. Xia, Z., Dudek, H., Miranti, C. K. & Greenberg, M. E. Calcium influx via the NMDA receptor induces immediate early gene transcription by a MAP kinase/ERK-dependent mechanism. *J. Neurosci.* **16,** 5425–5436 (1996).
19. Craig, A. M., Blackstone, C. D., Huganir, R. L. & Banker, G. Selective clustering of glutamate and GABA receptors opposite synaptic terminals releasing the corresponding neurotransmitters. *Proc. Natl Acad. Sci. USA* **91,** 12373–12377 (1994).
20. O'Brien, R. J. *et al.* The development of excitatory synapses in cultured spinal neurons. *J. Neurosci.* **17,** 7339–7350 (1997).
21. Gomperts, S. N., Carroll, R., Malenka, R. C. & Nicoll, R. A. Distinct roles for ionotropic and metabotropic glutamate receptors in the maturation of excitatory synapses. *J. Neurosci.* **20,** 2229–2237 (2000).
22. Cottrell, J. R., Dube, G. R., Egles, C. & Liu, G. Distribution, density, and clustering of functional glutamate receptors before and after synaptogenesis in hippocampal neurons. *J. Neurophysiol.* **84,** 1573–1587 (2000).
23. Balice-Gordon, R. J. & Lichtman, J. W. Long-term synapse loss induced by focal blockade of postsynaptic receptors. *Nature* **372,** 519–524 (1994).
24. Betz, W. J. & Bewick, G. S. Optical analysis of synaptic vesicle recycling at the frog neuromuscular junction. *Science* **255,** 200–203 (1992).
25. Li, Z. & Murthy, V. N. Visualizing post-endocytic traffic of synaptic vesicles at hippocampal synapses. *Neuron* **31,** 593–605 (2001).
26. Murthy, V. N., Schikorski, T., Stevens, C. F. & Zhu, Y. Inactivity produces increases in neurotransmitter release and synapse size. *Neuron* **32,** 673–682 (2001).
27. Bacci, A. *et al.* Chronic blockade of glutamate receptors enhances presynaptic release and downregulates the interaction between synaptophysin-synaptobrevin-vesicle-associated membrane protein 2. *J. Neurosci.* **21,** 6588–6596 (2001).
28. Paradis, S., Sweeney, S. T. & Davis, G. W. Homeostatic control of presynaptic release is triggered by postsynaptic membrane depolarization. *Neuron* **30,** 737–749 (2001).
29. Liao, D., Hessler, N. A. & Malinow, R. Activation of postsynaptically silent synapses during pairing-induced LTP in CA1 region of hippocampal slice. *Nature* **375,** 400–404 (1995).
30. Isaac, J. T. R., Nicoll, R. A. & Malenka, R. C. Evidence for silent synapses: implications for the expression of LTP. *Neuron* **15,** 427–434 (1995).

Supplementary Information accompanies the paper on *Nature*'s website (http://www.nature.com/nature).

Acknowledgements We thank E. Marban for the gift of the EGFP–IRES–Kir2.1 construct. We also thank the members of our laboratory for discussion. This work was supported by grants from the National Institutes of Health and the NSF. V.N.M. is a Sloan Foundation Fellow, a Pew Scholar, an EJLB Foundation Scholar and a National Alliance for Research on Schizophrenia and Depression (NARSAD) Young Investigator. J.B. is a Grable Investigator of NARSAD.

Competing interests statement The authors declare that they have no competing financial interests.

Correspondence and requests for materials should be addressed to V.N.M. (e-mail: vnmurthy@fas.harvard.edu).

Functional improvement of dystrophic muscle by myostatin blockade

Sasha Bogdanovich*†, Thomas O. B. Krag*†, Elisabeth R. Barton*, Linda D. Morris*, Lisa-Anne Whittemore‡, Rexford S. Ahima§ & Tejvir S. Khurana*

** Department of Physiology and Pennsylvania Muscle Institute, University of Pennsylvania School of Medicine, 3700 Hamilton Walk, Richards A-601, Philadelphia, Pennsylvania 19104-6085, USA*
‡ Musculoskeletal Sciences Department, Wyeth Research, Cambridge, Massachusetts 02140, USA
§ Division of Endocrinology, University of Pennsylvania School of Medicine, Philadelphia, Pennsylvania 19104, USA
† These authors contributed equally to this work

Mice[1,2] and cattle[3] with mutations in the myostatin (GDF8) gene show a marked increase in body weight and muscle mass, indicating that this new member of the TGF-β superfamily is a negative regulator of skeletal muscle growth. Inhibition of the myostatin gene product is predicted to increase muscle mass and improve the disease phenotype in a variety of primary and secondary myopathies. We tested the ability of inhibition of myostatin *in vivo* to ameliorate the dystrophic phenotype in the *mdx* mouse model of Duchenne muscular dystrophy (DMD)[4–8].

